NACACASE FILE COPY

RESEARCH MEMORANDUM

HYDRODYNAMIC INVESTIGATION

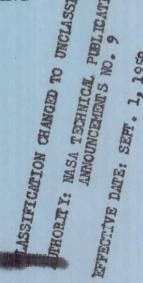
OF A MODEL OF A SUPERSONIC MULTIJET WATER-BASED

AIRCRAFT WITH ENGINES EXHAUSTING

FROM THE STEP

By Ulysse J. Blanchard

Langley Aeronautical Laboratory
Langley Field, Va.



NATIONAL ADVISORY COMMITTEE FOR AERONAUTICS

WASHINGTON

August 23, 1957



NATIONAL ADVISORY COMMITTEE FOR AERONAUTICS

RESEARCH MEMORANDUM

HYDRODYNAMIC INVESTIGATION

OF A MODEL OF A SUPERSONIC MULTIJET WATER-BASED

AIRCRAFT WITH ENGINES EXHAUSTING

FROM THE STEP

By Ulysse J. Blanchard

SUMMARY

The hydrodynamic characteristics of a multijet water-based aircraft capable of supersonic speeds and with jet engines exhausting through the step have been investigated. A 1/15-scale dynamic model, powered with hydrogen-peroxide jet motors was used for the investigation. The step engine exhausts considerably increased afterbody wetting and smoothwater resistance but had no significant effect upon longitudinal stability. Excess thrust was sufficient for the seaplane (full-scale) to take off in approximately 40 seconds and 4,700 feet. Longitudinal stability during smooth-water take-off and landing was satisfactory. During take-off, flap deflection should be delayed to speeds near take-off in order to avoid heavy flap wetting and associated high resistance. Landing characteristics were satisfactory for landing-contact trims at or above the sternpost angle. Spray characteristics in smooth water were good and engine inlets were clear of spray during taxiing and landing in waves up to 5 feet high. A jet-noise attenuation of 15 to 40 decibels resulted with static immersion of the step engine exhausts.

INTRODUCTION

The present investigation is part of a general research program to evaluate the hydrodynamic characteristics of water-based bomber configurations capable of flight at transonic and supersonic speeds. Previous investigations included tests of a wing-root-inlet configuration (ref. 1), a nose-inlet configuration (refs. 1 and 2), and a deck-inlet configuration (ref. 3). These configurations, which differed principally in the engine and inlet arrangements, conformed to area-rule requirements.





Along with this series of configurations, a planing-tail-hull design with the engines located in the root of a gull wing and the bomb bay located aft of the main step was proposed by the Bureau of Aeronautics. Results of hydrodynamic tests were reported in reference 4. In view of the good hydrodynamic characteristics of this planing-tail hull, further possibilities for attaining and improving the high-speed capabilities of the bomber series with such a configuration became of interest.

An appreciable reduction in frontal area was obtained by locating two of the four engines in the flotation part of the forebody. This low engine position was accomplished by placing the engine exhausts in the step below the afterbody. Results reported in references 5 and 6 indicated that by exhausting jet engines through the step, favorable aerodynamic lift and drag effects could be expected. A reduction in base drag of the deep step and an increase in the lift on the afterbody at supersonic flight speeds was expected from the presence of the engine exhausts in the step. In addition, the effect of jets exhausting under the afterbody on hydrodynamic characteristics was of general interest. An area distribution for a Mach number of 1.4 (ref. 3) was used and the volume and gross weight corresponded to a full-scale gross load of 200,000 pounds.

A hydrodynamic investigation was made in Langley tank no. 1 to determine the smooth-water resistance, spray characteristics, and take-off and landing stability of this configuration. A brief check of the rough-water spray during taxiing and landing in waves was made. Tests were conducted with and without power in order to determine the effect of the underwater jet exhausts upon important hydrodynamic characteristics. A brief evaluation of jet-noise attenuation when the jet exits were under water was made.

SYMBOLS

ъ	hull beam, ft
c	mean aerodynamic chord, ft
$^{\mathrm{C}}_{\mathrm{L}}$	aerodynamic lift coefficient, $\frac{L}{\frac{1}{2} \rho V^2 S}$
C_{m}	aerodynamic pitching-moment coefficient, $\frac{M}{\frac{1}{2} \rho V^2 S\overline{c}}$
$^{\mathrm{C}}_{\Delta_{\mathrm{o}}}$	gross-load coefficient, Δ_0

$$k = \frac{C_{\Delta_0}}{\left(\frac{l_f}{b_{\text{max}}}\right)^2}$$

$$K = \frac{c_{\Delta_0}}{\left(\frac{l_f + l_a}{b_{\text{max}}}\right)^2}$$

L total aerodynamic lift, lb

la afterbody length, ft

lf forebody length, ft

S wing area, sq ft

L.W.L. load water line, static water line at design gross weight

V carriage speed, ft/sec

w specific weight of water, 63.4 lb/cu ft for these tests

δe elevator deflection referred to stabilizer chord, positive when trailing edge is down, deg

δf flap deflection, positive when trailing edge is down, deg

δ_s stabilizer incidence referred to hull baseline, positive when trailing edge is down, deg

 Δ_0 gross load, 1b

Subscript:

max maximum

DESCRIPTION OF CONFIGURATION

A schematic drawing of the arrangement of the configuration is presented in figure 1. Pertinent dimensions and particulars are presented in table I. The hull lines of the configuration are presented in figure 2.



General Considerations

The gross load of 200,000 pounds, wing area of 2,000 square feet, and bomb load of 30,000 pounds were assumed. The bomb bay was located aft of the step at the airplane center of gravity in a similar arrangement to that of the planing-tail-hull-type configuration of reference 4. The wing was so located that 0.25c (normal c.g. location) was 1.3 beams behind the step. Four J-75 engines with afterburners were assumed to provide a maximum sea-level thrust of 94,000 pounds.

Engine location. - Two engines were located in the hull with a single nose inlet and step exits, and two engines were mounted in a nacelle on the vertical tail (fig. 1). This arrangement minimized accumulative cross-sectional area due to overlapping engine installations. The forward engines and their exits were angled down 5° and out 1.25° from the center line of the basic configuration.

The location of the rear engines on the vertical tail provided adequate spray clearance for the inlets and reduced the possibility of inlet flow interference from the hull and wing. A wedge-nose type of inlet was used for the basic nacelle design, as described in reference 7. The engines and nacelle were mounted parallel to the center line with engine exhausts behind the vertical tail.

Wing. - Dimensions of the wing are presented in table I. Wing-tip floats were not used due to their drag contribution at supersonic speeds (ref. 1). The assumption was made that auxiliary devices such as retractable skis and inflatable air cells would be used for dynamic and static transverse stability.

Planing bottom. - A high-length-beam-ratio planing-tail hull with planing surfaces similar in layout and plan form to those of the configuration of reference 4 was used. The forebody beam and dead rise were governed by the installation of the engines in the lower portion of the hull. The long, full-width plan form of the afterbody chines (fig. 2) was provided to insure spray control in the region of the aft engine inlets. The entire planing bottom had sharp chines, with dead rise and horizontal chine flare on the forebody and simple dead rise on the afterbody. The forebody in the region of the step and engine exits was filleted as much as possible to reduce blunt base areas. The length of the hull was determined by aerodynamic considerations of fineness ratio which were compatible with a high-length-beam-ratio hull.

Tail group. - A high-horizontal-tail position was used to provide spray clearance. Dimensions of the tail group are presented in table I.





Cross-Sectional-Area Distribution

The curve of the net total cross-sectional area for a Mach number of 1.4 and the contributions of the various components are presented in figure 3. The area distributions were developed as described in references 3 and 8 for moderate supersonic speeds. From hot-jet test results obtained in the Langley 8-foot transonic tunnel, the hot jets were estimated to expand from 8.9 square feet per engine at the exit to an effective or displacement area of 12.9 square feet aft of the exit. Since drag is sensitive to the change in area and this change occurs at the critical middle section of the area distribution, 4.0 square feet per engine was assumed to be the contribution to the total cross-sectional area made by the hot jet (fig. 3). This jet displacement effect was assumed to extend aft from the exits but with diminishing influence, becoming zero approximately 40 feet (full-scale) from the exits.

The large reduction in hull cross-sectional area aft of the deep step minimized the additive effect of hull and wing cross sections. The longitudinal spacing of the engines and wing and the housing of the forward engines in the flotation portion of the forebody resulted in essentially minimum frontal area. With an equivalent free-stream tube area of 80 percent of the inlet area subtracted for the mass flow through the ducts, a maximum net cross-sectional area (including jet effect) of 126.5 square feet was obtained. The fineness ratio of the equivalent body of revolution was 12.8.

Tank Model

Photographs of the 1/15-scale powered dynamic model, Langley tank model 333, are presented in figure 4. The hull was constructed of fiber glass and heat-resistant plastic in order to permit the use of a hydrogen-peroxide jet-power system. The wing and tail surfaces were of conventional wooden construction covered with silk and coated with peroxide-compatible paint. All metal accessories were made of aluminum or stainless steel, which are compatible with concentrated hydrogen peroxide. The pitching moment of inertia of the complete model was 5.34 slug-feet².

Leading-edge, 0.15-chord slats were used to prevent the premature wing stall usually encountered at the low Reynolds numbers of tank tests. Full-span, 0.30-chord, single-slotted flaps were used on the wing with fixed angles of deflection of 0° and 40°. The stabilizer deflection could be varied from 5° to -15° and the elevator deflection, from 30° to -20°.

Electric contacts were located on the hull keel at the bow, step, and sternpost. The contacts indicated when these portions of the hull





were in contact with the water and also were used to release a trim brake during landing tests.

Scale thrust of 7 pounds for each of the two forward engines was simulated by hydrogen-peroxide motors mounted in the step. Plastic ducts housed the motor and shroud assembly (see fig. 5). The open inlet and ducts supplied cooling air and the stainless-steel shrouds acted as heat suppressors around the motors. Only a negligible change in thrust with speed was noted in the speed range of the tests.

The hydrogen-peroxide motor had an orifice head, a decomposition chamber, and a supersonic convergent-divergent nozzle on the aft end of the chamber. The orifice diameter at the head of the chamber was 0.052 inch. A catalyst bed, approximately 2.5 inches long, was made of alternate silver and stainless-steel screen discs packed into the 0.600-inch-diameter decomposition chamber. The nozzle-throat diameter was 0.210 inch and the nozzle-exit diameter, 0.345 inch. Design throat pressure was approximately 210 pounds per square inch and maximum thrust capacity of the motor was approximately 10.5 pounds.

The fuel was concentrated hydrogen peroxide which decomposed upon contact with the silver-screen catalyst bed of the motor and produced a high-velocity jet exhaust. Fuel was introduced through a 3/16-inch (inside diameter) flexible dacron-covered vinyl plastic tube from a supply reservoir and control console mounted on the towing carriage.

Jet-exit modifications which altered the direction of the jet-exhaust stream from the step are shown in figure 6. These steel tubes, approximately 4 inches long (model size), were installed at various angles. On model 333A, the deflector tubes were tilted up 10°, model 333B out 10°, and model 333C out 30° with respect to the basic engine alinement.

APPARATUS AND PROCEDURES

The investigation was made in Langley tank no. 1, which is described in reference 9. The apparatus and procedures used are described in reference 10 and are similar to those used for the investigation described in reference 4.

The aerodynamic lift and pitching-moment characteristics shown in figure 7 were determined for the normal center-of-gravity location $(0.25\bar{c})$. The height of the model above the water was adjusted for each trim so that the lowest point on the model was just clear of the water. Aerodynamic tests were made with and without power simulated for the forward engines only. The power-on moment data were corrected for the computed moment associated with the threat of the rear engines.



All hydrodynamic tests were made with the center of gravity located at 0.25c and a gross load corresponding to 200,000 pounds, full-scale, except rough-water landings, which were made at a gross load of 160,000 pounds. All tests were made with and without power except landings and rough-water taxi runs, which were made power off only. During powered tests, thrust for the forward engines only was simulated and the pitching moment associated with the thrust of the rear engines was applied by means of a weight moment. For smooth-water tests, the model was pivoted at the center of gravity and had freedom in only trim and rise. For rough-water tests, the model also had fore and aft freedom. Trim was the angle between the forebody keel at the step and the undisturbed water surface.

The trim and resistance, including air drag, power off and power on, of the complete model were determined for a range of constant speeds with the model free to trim. In order to obtain power-on resistance, scale thrust of the engines was set before each run and added to the gross resistance measured during the run. The thrust of the engines was set with the model at rest and clear of the water at zero trim. The constant-speed data were obtained for a flap deflection of 0° and speeds up to approximately 150 knots (full-scale), and for a flap deflection of 40° and speeds from approximately 70 knots to take-off. Resistance with the wing removed was determined at fixed trims, speeds, and approximate loads corresponding to those obtained for the complete model.

Simulated take-off runs were made at an acceleration of 4 ft/sec^2 , which approximated that acceleration which would result from the available excess thrust. Take-off runs were made in two parts, with a flap deflection of 0° to a speed of approximately 140 knots, and with a flap deflection of 40° from 70 knots to take-off. Take-offs were made for a range of fixed stabilizer-elevator settings.

Landings were made with 40° flap deflection for a range of landing-contact trims. With the model flying at the desired landing trim, the carriage was decelerated at various uniform rates, allowing the model to glide onto the water. The model was held at the desired landing trim by the trim brake until contact with the water surface.

Spray characteristics in smooth water and in waves were determined from visual observations, photographs, and motion pictures. Smoothwater spray was studied during free-to-trim resistance and landing tests. Spray characteristics in waves were determined during landings and accelerated taxi runs (2 ft/sec²). Since the model was not powered during taxi runs, fore-and-aft freedom was maintained by approximating the horizontal thrust component with a long-rubber-band arrangement described in reference 11.





Jet-noise attenuation tests were conducted statically and out of doors in order to eliminate carriage noises and sound reflections which might occur during operation in the tank. The model was lowered into the water from a height of 2 feet above the water and sound was recorded on a sound track from 5 positions equidistant from the model and ranging from front to rear. The sound intensities were then measured from the sound track with a sound-level meter and the change in intensity due to jet immersion was determined.

RESULTS AND DISCUSSION

Spray Characteristics

Smooth water. Typical bow and stern photographs of the smoothwater spray with and without power are shown in figure 8 for the complete model. The forward inlet was well clear of spray at all times. No spray entered the rear inlets although light spray struck the aft lower surface of the rear nacelle at speeds from 60 to 95 knots. At low speeds fine spray from the forebody wake wetted the upper surface of the wing and heavy spray impinged upon the lower surface. The flaps became clear of heavy spray at a speed of approximately 115 knots. The horizontal tail was clear of spray at all speeds. In general, the significant change in spray with the application of power was the deflection of the forebody wake onto the afterbody sides (see fig. 8(b)) and the extensive atomizing and acceleration of the spray by the jet exhaust.

Rough water. - A brief rough-water spray investigation indicated that during landings the inlets and horizontal tail were clear of spray in waves up to 5 feet in height and 270 feet in length. In waves 7.5 feet high and 270 feet long the bow dug into the wave at low speeds and solid water entered the forward inlets.

During slow accelerated taxiing runs in waves 270 feet long the inlets were clear of spray until the 7.5-foot-wave height was reached, when solid water entered the forward inlet at low speeds and light spray entered the rear inlets at high speed. In a long wave (450 feet), the inlets were clear at the 7.5-foot-wave height; however, light spray struck the horizontal tail. Wing and flap wetting increased generally with increase in wave height.

Resistance and Stability, Constant Speed

Power off.- The total resistance and corresponding trims for 0° and 40° flap deflections, without power, are presented in figure 9. Without





power and with 0° flap deflection (fig. 9(a)), the resistance increased with speed to approximately 62 knots, at which speed a minimum grossload—total-resistance ratio of 3.4 was obtained. With further increase in speed, the resistance decreased as the afterbody and wing wetting decreased. At a speed of approximately 110 knots the resistance again increased and a yawing instability developed. The data indicate a discontinuity in the trim curve at this point. At this speed the forebody wake was observed to have moved inboard and an unsymmetrical and intermittent flow began attaching to the afterbody sides and bottom. A typical condition during yawing instability is shown in figure 8(b) (V = 126.8 knots).

In this same speed region of approximately 110 knots (fig. 9(a)), longitudinal instability was encountered at the high stabilizer-elevator deflection ($\delta_{\rm S}=-10^{\circ}$; $\delta_{\rm e}=-20^{\circ}$). This instability was characterized by a constant-amplitude rocking motion between the two planing surfaces, rather than the divergent type generally associated with upper-limit porpoising. The amplitude of oscillation increased with increase in trim. At very high speeds (near 150 knots) the resistance and trim decreased rapidly and the model became stable. At these high speeds and low trims the afterbody was clear of spray or attaching flow.

At speeds below 115 knots, deflection of the flaps to 40° (fig. 9(b)), increased resistance considerably from that for no flap deflection (fig. 9(a)) due to heavy flap wetting. At speeds above 115 knots, the flap became clear of heavy spray and the total resistance for both flap deflections (0° and 40°) was not very different. Trims, however, were lower with 40° flap deflection, and regions of longitudinal instability similar to that noted for a flap deflection of 0° are indicated. No significant yawing instability was noted in this case.

Power on.- With power and 0° flap deflection (fig. 10(a)), a minimum gross-load—total-resistance ratio of 2.8 was obtained, as compared to 3.4 without power. At speeds from approximately 25 to 115 knots, the power-on resistance was considerably higher than without power. At speeds near 115 knots, the power-off and power-on resistance were generally the same. At speeds near getaway, however, the resistance with power on tended to be higher than that with power off, principally because power increased the amount and velocity of spray striking the afterbody.

The yawing instability encountered with 0° flap deflection, power-off (fig. 9(a)), was reduced considerably with the application of power (fig. 10(a)). The discontinuity in the trim at high speed for 0° flap deflection occurred at a lower speed with power, 85 knots, than without power, 115 knots. Deflection of the horizontal tail had no significant





effect on trim until the point of trim discontinuity was reached in either case. The region of longitudinal instability is shown in figure 10(a).

With power and a 40° flap deflection (fig. 10(b)), the resistance was generally higher than that with a flap deflection of 0° throughout the high-speed range and considerably higher than power-off resistance. The flaps became clear of heavy spray at speeds between 110 and 115 knots.

The resistance and trim for a typical powered take-off run are presented in figure 11. This take-off is based on the assumption that the flaps would not be fully deflected until a speed of approximately 115 knots to avoid heavy wetting from spray. Excess thrust is available for acceleration throughout the speed range and the computed take-off time and distance are 40 seconds and 4,700 feet (full-scale).

Wing removed. The cause of increases in resistance with the application of power (jets exhausting through the step) can be best illustrated by the photographs in figure 12, taken during resistance tests with the wing removed. The drastic change of flow in the afterbody region with power on is obvious. Separation of flow from the chines and the afterbody clearance relative to the forebody wake are completely changed when power is applied and the forebody wake is drawn inward and redirected at increased velocity upon the afterbody bottom and sides. The area beneath the afterbody becomes completely filled with a high-velocity stream of water directed rearward along the afterbody. Further evidence of this large change in flow can be seen in the spray photographs shown in figure 8.

Resistance data, power off and power on, measured during tests with the wing removed are presented in figure 13. For comparison, resistance of the complete model, power off and power on, is included (dashed lines) in the figure. With power on, the change in resistance with and without the wing is less than that obtained with power off. This difference would be expected on the basis of the stern spray photographs in figure 8(b), which show that with application of power the wetted-wing area is drastically reduced by the large change in flow pattern induced by the jet exhausts. With power, the wetting is almost entirely directed upon the hull bottom and sides and wetting persisted to very high speeds.

Jet exhaust deflection.— It was believed that by directing the jet blasts in some advantageous direction, within practical limits, afterbody wetting could be reduced with a consequent reduction in power-on resistance. The resistance data for the three jet deflections shown in figure 6 are presented in figure 14, along with a dashed-line curve representing the data obtained with the basic configuration. Deflecting the jets up 10° (model 333A) in an attempt to blow the water off the



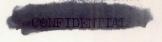
afterbody bottom resulted in an increase in total resistance when compared with that of the basic model. This increase in resistance indicated that possibly even more water was being directed upon the afterbody. The increase was practically constant over most of the speed range. Deflecting the jets outward 100 (model 333B) resulted in no significant change in resistance from that of the basic arrangement. A larger deflection was considered impractical but since no visible change in flow pattern had been noted with the two previous attempts, an outward deflection of 30° (model 333C) was investigated as an all-out attempt to alter the flow. A particularly large increase in resistance was noted just past hump speed and is attributed to a heavy wetting of the wing caused by the jet stream, which, for this configuration, was being directed outward and along the wing span. At intermediate and high speeds the trend of the resistance curve and its magnitude were generally the same as that obtained without power. At these speeds, for this configuration, the afterbody was observed to become clear of heavy water flow once again. It can be surmised that practical jet deflections would not improve the resistance over that obtained with the basic configuration.

Engine starting. - From observations and data obtained during the resistance tests, a possible solution to the problem of starting the forward engines can be presented. During power-off tests the step region vented at a speed of approximately 25 knots. Sufficient excess thrust would be available from operation of the rear engines to accelerate to this speed, at which point watertight exit doors could be opened and the forward engines started.

Take-Off Stability

The variation of trim with speed during accelerated runs simulating take-off for flap deflections of 0° and 40° is shown in figure 15 with-out power and in figure 16 with power. Generally, the characteristics of the trim tracks were similar. Approximate trim limit and take-off speed curves derived from the trim track records also are shown. No lower trim limit of stability was encountered when operating at this design center-of-gravity position and available aerodynamic pitching moment. At high trims and speeds a trim oscillation similar to that encountered during constant-speed resistance was noted. Upon entering this region of instability, the amplitude of the trim oscillation increased with stabilizer-elevator deflection. The yawing instability during take-off was of little concern, since the model accelerated through the region before any significant oscillations occurred.

Study of the trim tracks during powered take-offs with flap deflections of 0° and 40° (fig. 16) shows that deflection of the flaps just after hump speed (approximately 70 knots) would permit trimming below





the upper limit, and that by maintaining low trim to a speed of approximately 110 knots, the pilot could then increase trim and thereby make a stable take-off. However, the increased resistance due to flap wetting (see resistance curves) near hump speed would increase the time and distance for take-off. The best trim track for 0° flap deflection (solid line) and several trim tracks for 40° flap deflection (dashed line) are shown in figure 17. These results show that with available aerodynamic trimming moment, a relatively stable (1° trim oscillation) take-off could be made by delaying full-flap deflection to a speed of approximately 115 knots. Low trim would be maintained until flaps are deflected, after which a stable take-off could be made which would be representative of the typical take-off resistance curve in figure 11.

Landing Stability

Figure 18 presents typical oscillograph records showing trim, rise, and speed during landings in smooth water. Landings at trims below the sternpost angle (7.6°) resulted in a sharp increase in trim subsequent to the initial contact (fig. 18(a)); also, landings at trims above the sternpost angle resulted in a sharp decrease in trim subsequent to initial contact (fig. 18(c)). Although the large trim changes were quickly damped, small trim oscillations persisted through a large part of the landing runout as the fore-and-aft planing surfaces sought trim equilibrium.

The maximum variation in trim and rise as well as the number of rebounds during landings in smooth water are presented in figure 19. For trims at initial contact below the sternpost angle, the maximum amplitude of trim oscillations was approximately 6.5° and the model tended to bounce off the water once. At contact trims above the sternpost angle, the maximum amplitude of trim oscillation was approximately 4.5° and the model remained on the water after contact. The maximum amplitudes of rise oscillation remained practically constant regardless of landing trim. Only at the highest landing trim was there a significant increase in rise amplitude. The overall landing behavior appeared acceptable.

Jet Noise

During tank tests, a considerable reduction in jet-noise level was observed at low taxi speeds and at rest when the step-engine exits were under water. When measured out of doors, the decrease in sound level at maximum draft from the sound level with the model clear of the water varied from 15 decibels at the front to a maximum of 40 decibels at the rear.





CONCLUDING REMARKS

The hydrodynamic characteristics of a supersonic multijet waterbased aircraft with jet exits in the step have been investigated. The jets exhausting through the step generally resulted in considerable increase in afterbody wetting and hence increased resistance, but had no significant effect upon longitudinal stability. A minimum grossload -resistance ratio of 2.8 was obtained with power. Excess thrust was sufficient for a take-off in approximately 40 seconds and 4,700 feet. Longitudinal stability during smooth-water take-off and landing was satisfactory. During take-off, flap deflection should be delayed to speeds near take-off because of increased resistance due to flap wetting at intermediate speeds. During landing, large initial trim changes at contact were quickly damped. Amplitudes of subsequent trim and rise oscillation were relatively small, especially for landing contact trims near or above sternpost angle. The spray characteristics in smooth water were good and rough-water operation with spray-free inlets would be possible in waves up to 5 feet high. A jet-noise attenuation of 15 to 40 decibels resulted with static immersion of the step-engine exhausts.

Langley Aeronautical Laboratory,
National Advisory Committee for Aeronautics,
Langley Field, Va., June 6, 1957.





REFERENCES

- 1. Olson, Roland E., and Bielat, Ralph P.: An Aerodynamic and Hydrodynamic Investigation of Two Multijet Water-Based Aircraft Having Low Transonic Drag Rise. NACA RM L55Alla, 1955.
- 2. McKann, Robert E., and Coffee, Claude W.: Limited Hydrodynamic Investigation of a 1/15-Size Model of a Modified Nose-Inlet Multijet Water-Based Aircraft. NACA RM L55J19, 1956.
- 3. Bielat, Ralph P., Coffee, Claude W., and Petynia, William W.: Aero-dynamic and Hydrodynamic Characteristics of a Deck-Inlet Multijet Water-Based-Aircraft Configuration Designed for Supersonic Flight. NACA RM L56HOl, 1956.
- 4. Morse, Archibald E., Jr., Woodward, David R., and Blanchard, Ulysse J.:
 An Investigation of the Hydrodynamic Characteristics of a Dynamic
 Model of a Transonic Seaplane Design Having a Planing-Tail Hull.
 NACA RM L56C28a, 1956.
- 5. Wasserbauer, Joseph F., and Englert, Gerald W.: Interaction of an Exhaust Jet and Elementary Contoured Surfaces Located in a Supersonic Air Stream. NACA RM E56A16, 1956.
- 6. Falanga, Ralph A., and Judd, Joseph H.: Flight Investigation of the Effect of Underwing Propulsive Jets on the Lift, Drag, and Longitudinal Stability of a Delta-Wing Configuration at Mach Numbers From 1.23 to 1.62. NACA RM L55II3, 1955.
- 7. Carmel, Melvin M., and Fischetti, Thomas L.: A Transonic Wind-Tunnel Investigation of the Effects of Nacelles on the Aerodynamic Characteristics of a Complete Model Configuration. NACA RM L53F22a, 1953.
- 8. Whitcomb, Richard T.: Some Considerations Regarding the Application of the Supersonic Area Rule to the Design of Airplane Fuselages.

 NACA RM L56E23a, 1956.
- 9. Truscott, Starr: The Enlarged N.A.C.A. Tank, and Some of Its Work. NACA TM 918, 1939.
- 10. Olson, Roland E., and Land, Norman S.: Methods Used in the NACA Tank for the Investigation of the Longitudinal-Stability Characteristics of Models of Flying Boats. NACA Rep. 753, 1943 (Supersedes NACA WR L-409).
- 11. Mottard, Elmo J.: A Brief Investigation of the Effect of Waves on the Take-Off Resistance of Complete NACA RM L56B09, 1956.





TABLE I.- CHARACTERISTICS OF CONFIGURATION

	General:				
	Design gross weight, lb				200,000
	Wing area, sq ft				2,000
	Design wing loading, lb/sq ft				100
	Engines, J-75 with afterburners				. 4
	Total net sea-level thrust (with afterburners), lb				94,000
	Design thrust-weight ratio				0.47
	Manage				
1	Wing: Airfoil section:				
				*** ~ *	(1100)
	Root				64A206
	50 percent semispan to tip			NACA	
	Aspect ratio				89.5
	Taper ratio				4.0
	Dihedral, deg		•		-2.0
	Sweepback (0.25ē), deg				45
	Root incidence, deg				1.25
	Length of \bar{c} , ft				26.5
	Hull station O to leading edge of \bar{c} , ft				76.3
	Position of 0.25c above baseline, ft				13.5
	Total of the above saterine, it		 ,		1).)
1	Morizontal tail:				
	Airfoil section		. 1	NACA	65A006
	Span, ft				35.2
	Area, sq ft				310
	Aspect ratio				4.0
	Taper ratio				0.3
	Dihedral, deg				0.9
	Sweepback (0.25c), deg				45
	Distance between 0.25c of wing and 0.25c of tail, ft				75.2
	Height above baseline, ft				35.6
					,,,,,
V	fertical tail:				
	Airfoil section	 	 . 1	VACA	65-006
	Aspect ratio				1.13
	Sweepback (0.25c), deg	 			47
E	full:				
	Maximum beam at chines, ft	 	 		10.8
	Maximum width, ft	 			12:1
	Maximum height, ft	 			19.3
	Length:				-,.,
	Overall, ft	 			153.25
	Forebody (chines at bow to step point), ft	 			61.6
	Afterbody, ft	 			84.4
	Step:				
	Type	 			Pointed
	Depth at keel, ft				5.5
	Depth at keel, percent beam				51
	Deadrise, forebody				Warped
	Deadrise, afterbody				Warped
	Afterbody keel angle, deg				3.86
	Sternpost angle, deg				7.6
	Center of gravity (0.25c) aft of step, ft				13.98
	Center of gravity above baseline, ft				12.5
	Angle to vertical of line joining step to center of gravity, deg				48.4
	Hull volume (volume of ducts subtracted), cu ft				8,425
	Hull surface area, sq ft				4,767
	$l_{ extsf{f}}$				
	b _{max}				5.7
	"max				
	la				7.8
	b _{max}	•			1.0
	l _f				
					0.73
	la l				
	$\frac{l_{\rm f}+l_{\rm a}}{l_{\rm c}}$				17 6
	b _{max}				13.5
					2.48
					2.40
	K				0.014
	k				0.076
1750					
A:	rea distribution:				
	Maximum net cross-sectional area, sq ft				126.5
	Equivalent-body maximum diameter, ft				12.7
	Length, ft				162.5
	Equivalent body fineness ratio				12.5
	Maximum net area				0.063
	Wing area Position of maximum cross section of equivalent body in terms of body length, percent				
					46
	Total surface area, sq ft				9,871



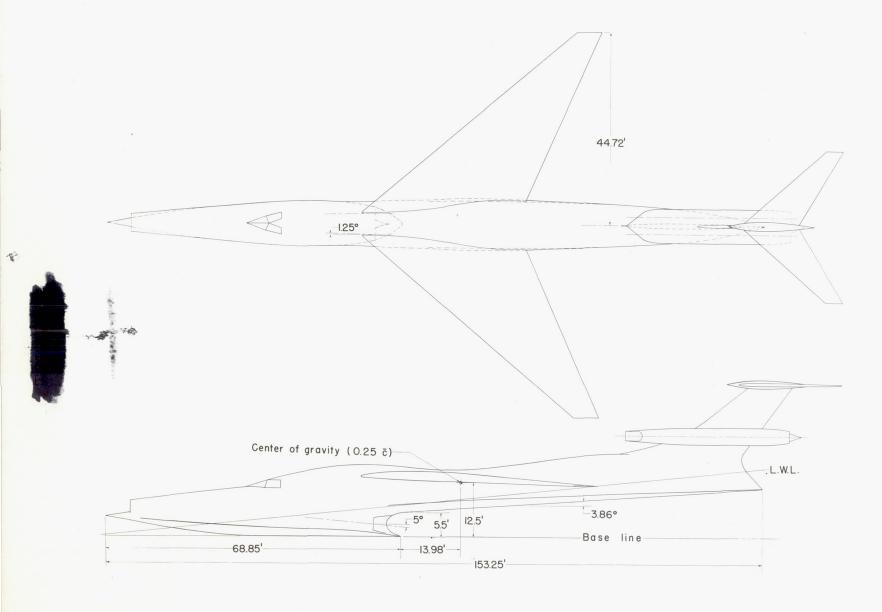


Figure 1.- Arrangement of step-exhaust configuration.

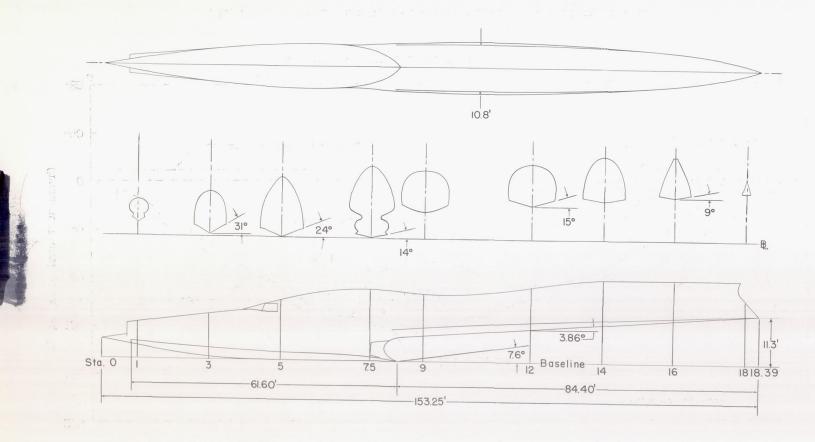


Figure 2.- Layout of step-exhaust-configuration hull.

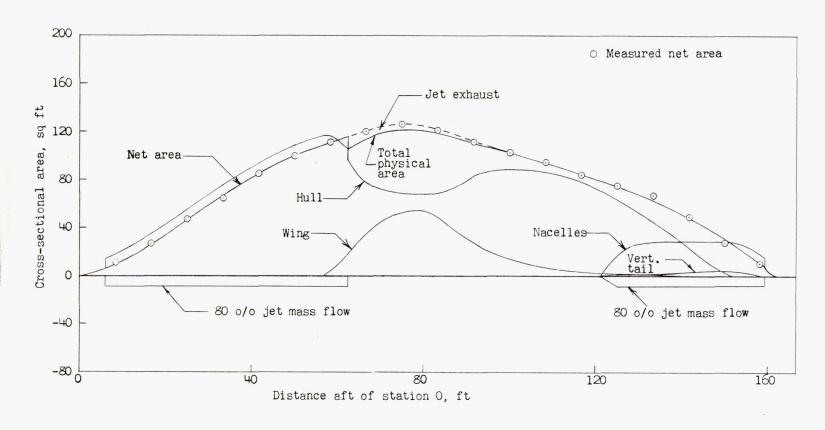
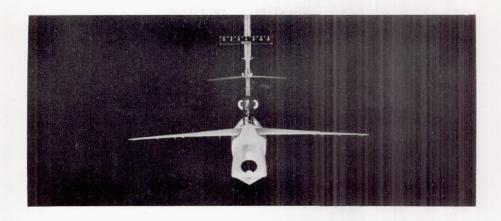
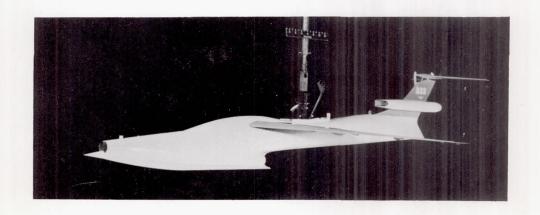


Figure 3.- Cross-sectional-area curve of configuration.

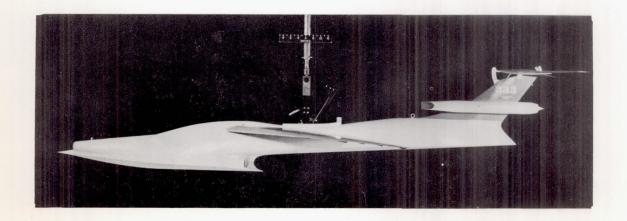




(a) Front view.



(b) Three-quarter front view.



(c) Side view.

Figure 4.- The 1/15-scale Langley tank model 333. L-92031



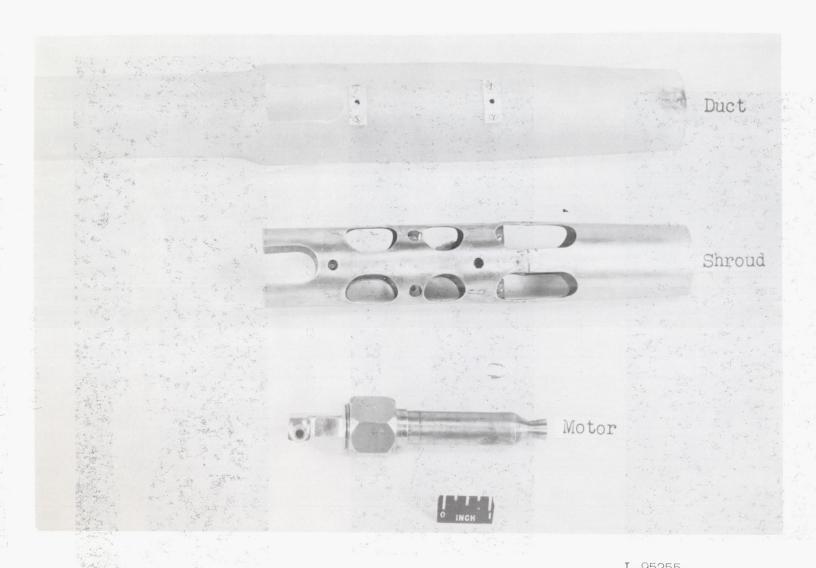
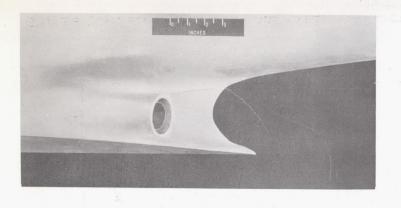
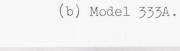


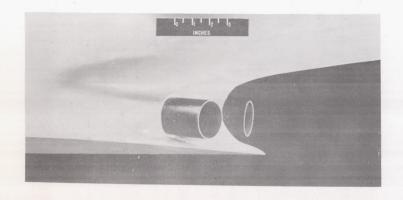
Figure 5.- Duct, shroud, and motor assembly. Langley tank model 333.



INCHES

(a) Model 333 basic.







(c) Model 333B.

(d) Model 333C. L-57-1620

Figure 6.- Jet-exit modifications. Langley tank model 333.

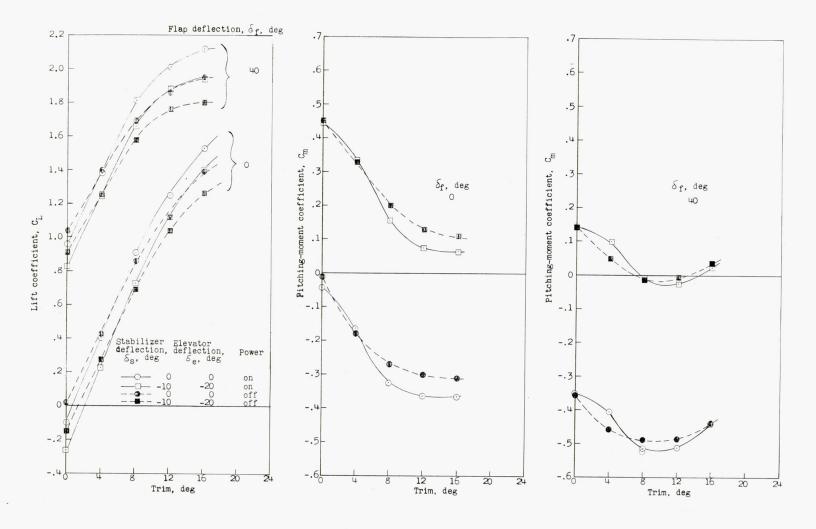
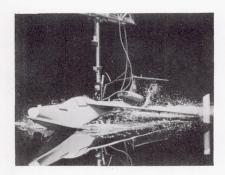
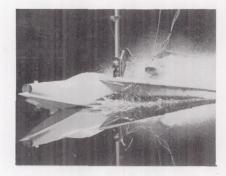


Figure 7.- Aerodynamic lift and pitching-moment characteristics with the normal center-of-gravity location (0.25 \bar{c}).

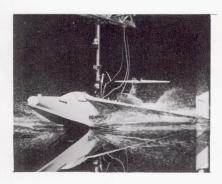




Speed, 34.6 knots; trim, 7.2°.



Speed, 35.3 knots; trim, 6.4°.



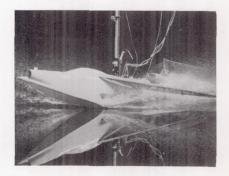
Speed, 57.8 knots; trim, 9.2°.



Speed, 58.2 knots; trim, 9.2°.



Speed, 63.5 knots; trim, 9.6°. Speed, 69.0 knots; trim, 10.0°. Power off



Power on

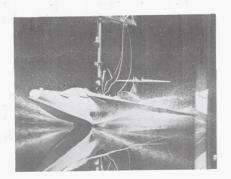
(a) Bow view.

L-57-1609

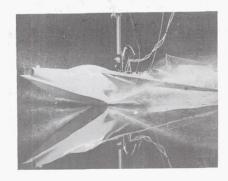
Figure 8.- Spray photographs of complete model during power-on and power-off resistance runs. $\Delta_0 = 200,000$ pounds; $\delta_f = 0^{\circ}$.



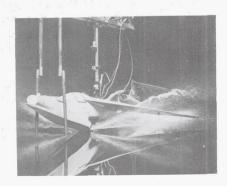




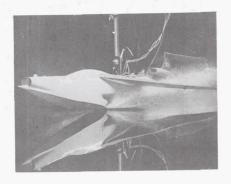
Speed, 80.5 knots; trim, 9.9°.



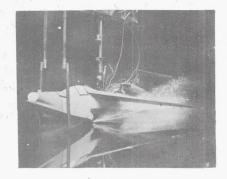
Speed, 80.7 knots; trim, 10.0°,

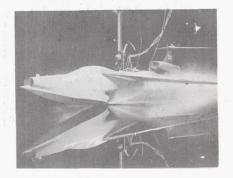


Speed, 104.4 knots; trim, 9.8°.



Speed, 103.4 knots; trim, 7.8°.





Speed, 126.8 knots; trim, 7.4°. Speed, 128.2 knots; trim, 7.6°.

(a) Concluded. L-57-1610

Figure 8. - Continued.

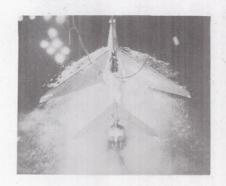


S





Speed, 34.6 knots; trim, 7.2°.



Speed, 35.3 knots; trim, 6.4°.



Speed, 57.8 knots; trim 9.2°.



Speed, 58.2 knots; trim, 9.2°.



Power off



Speed, 63.5 knots; trim, 9.6°. Speed, 69.0 knots; trim, 10.0°. Power on

(b) Stern view.

L-57-1611

Figure 8.- Continued.







Speed 80.5 knots; trim, 9.9°.



Speed, 80.7 knots; trim, 10.0°.



Speed, 104.4 knots; trim, 9.8°.



Speed, 103.4 knots; trim, 7.8°.



Speed, 126.8 knots; trim, 7.4°.

Power off



Speed, 128.2 knots; trim, 7.6°.

Power on

(b) Concluded.

L-57-1612

Figure 8.- Concluded.



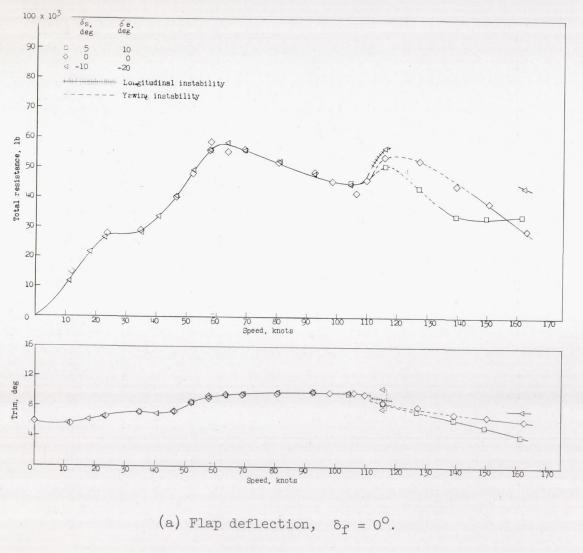
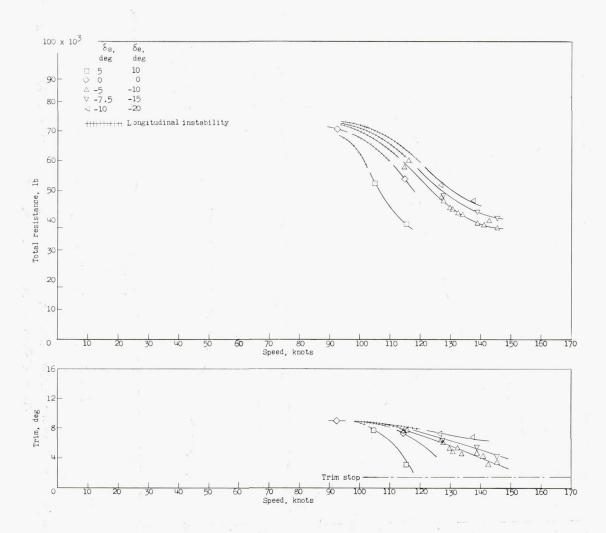


Figure 9.- Variation of free-to-trim total resistance and trim with speed in smooth water. $\Delta_0 = 200,000$ pounds; power off.

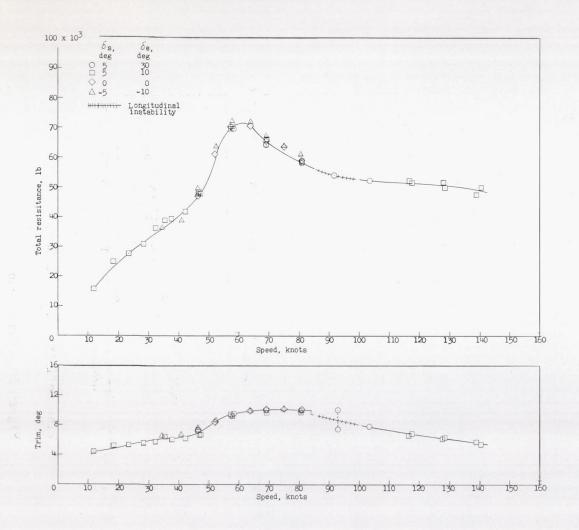


(b) Flap deflection, $\delta_f = 40^{\circ}$.

Figure 9.- Concluded.

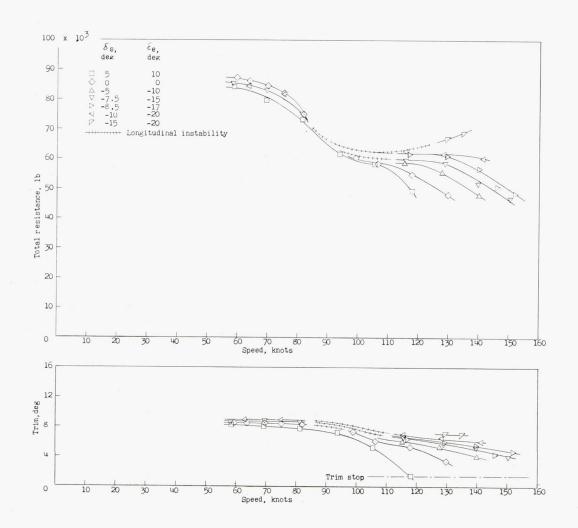






(a) Flap deflection, $\delta_f = 0^{\circ}$.

Figure 10.- Variation of free-to-trim total resistance and trim with speed in smooth water. $\Delta_0 = 200,000$ pounds; power on.



(b) Flap deflection, $\delta_{f} = 40^{\circ}$.

Figure 10.- Concluded.

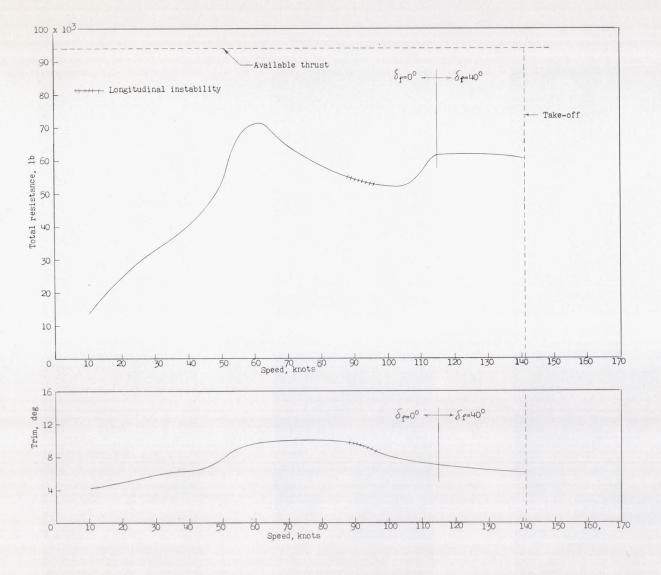
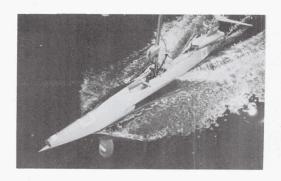


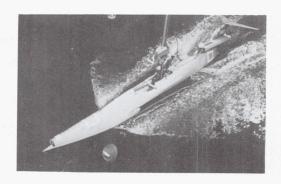
Figure 11.- Typical take-off trim track and total resistance. Δ_0 = 200,000 pounds; power-on; take-off time, 40.0 seconds; take-off distance, 4,700 feet.





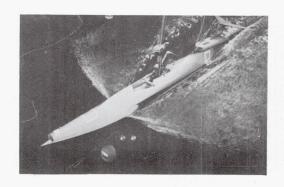


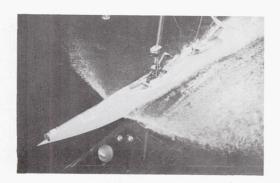
Speed, 34.9 knots; trim, 6.5°.





Speed 41.3 knots; trim, 7.0 °





Speed, 58.0 knots; trim, 9.0 .

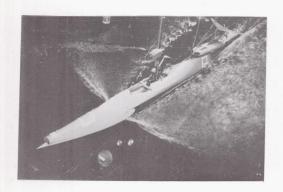
(a) Power off.

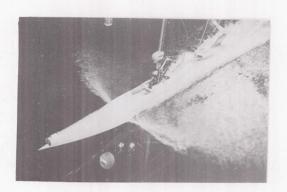
(b) Power on. L-57-1613

Figure 12.- Spray photographs of model during resistance tests of hull alone.

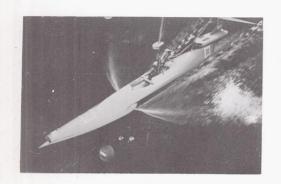


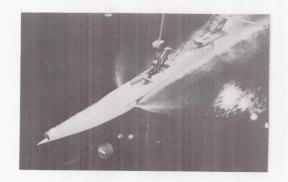






Speed, 63.3 knots; trim, 9.5°.





Speed, 117.0 knots; trim, 6.5°.

(c) Power off.

(d) Power on.

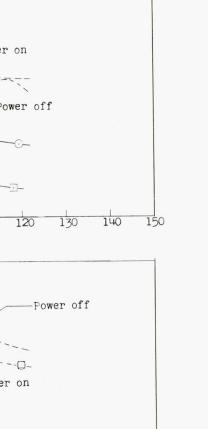
L-57-1614

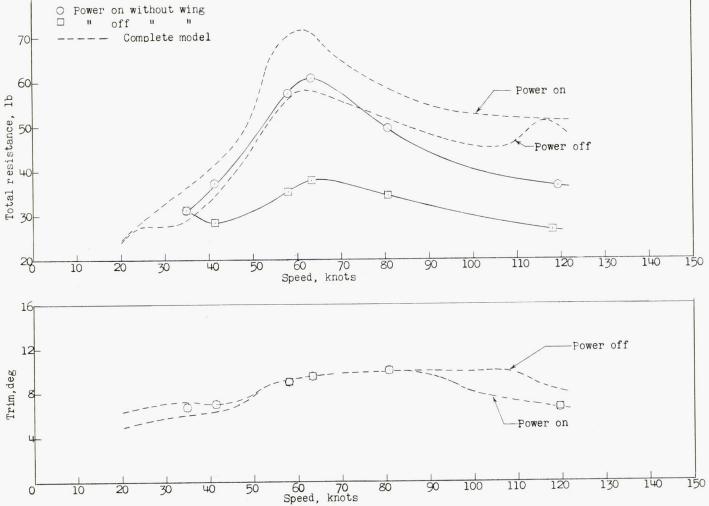
Figure 12.- Concluded.





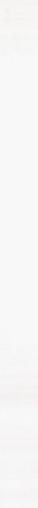
NACA RM L57F20





80 x 10³-

Figure 13.- Variation of total fixed-trim resistance for the hull alone with speed in smooth water. Power on and power off; $\delta_{\rm S}$ = $5^{\rm O}$; $\delta_{\rm e}$ = $10^{\rm O}$.



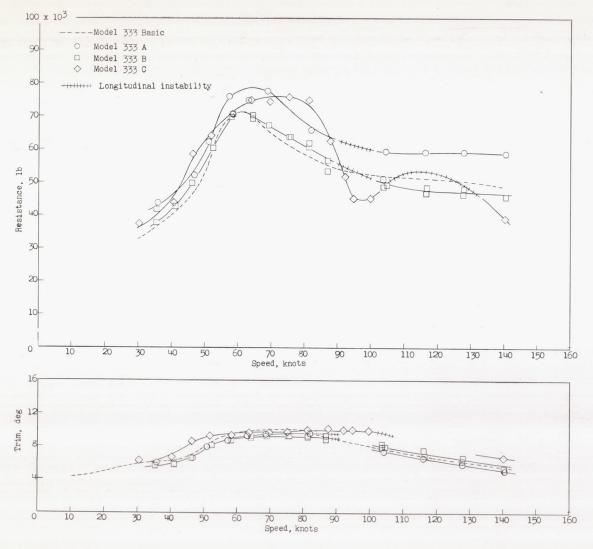


Figure 14.- Variation of free-to-trim total resistance and trim with speed for various jet deflections. $\Delta_{\rm O}$ = 200,000 pounds; $\delta_{\rm f}$ = 0°; $\delta_{\rm S}$ = 5°; $\delta_{\rm e}$ = 10°; power on.

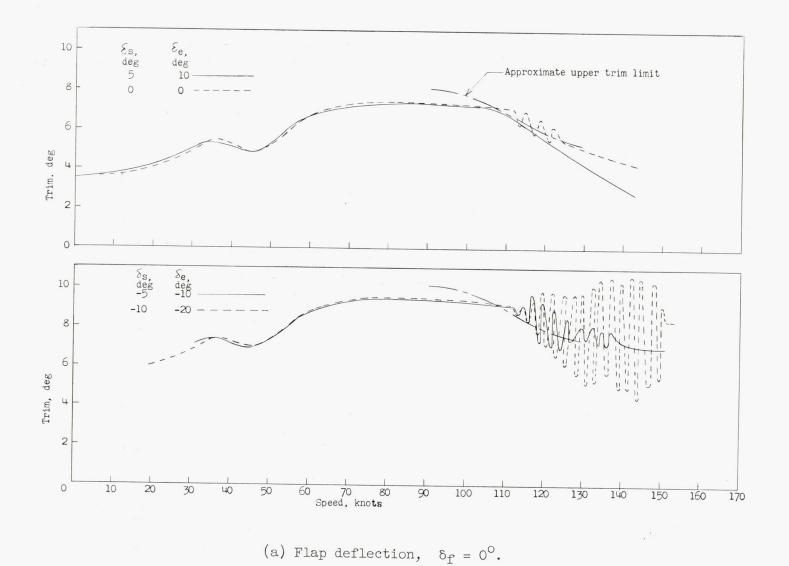
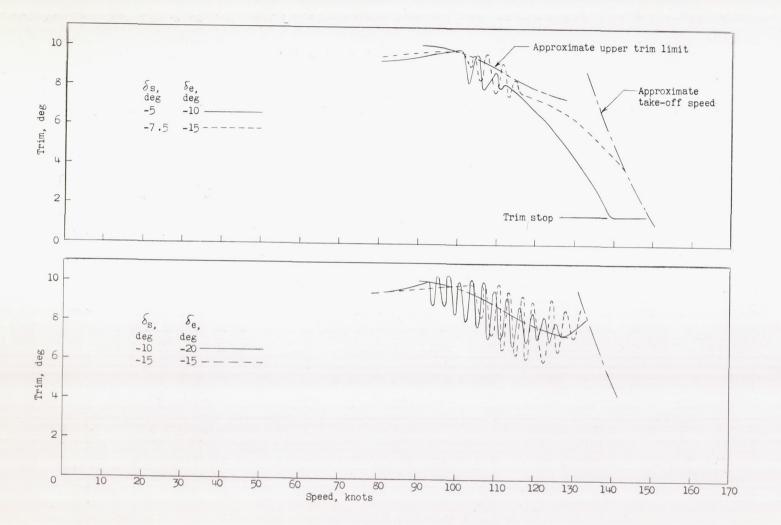


Figure 15.- Variation of trim with speed during take-off in smooth water. Δ_0 = 200,000 pounds; power off.

7



(b) Flap deflection, $\delta_{\text{f}} = 40^{\circ}$.

Figure 15.- Concluded.

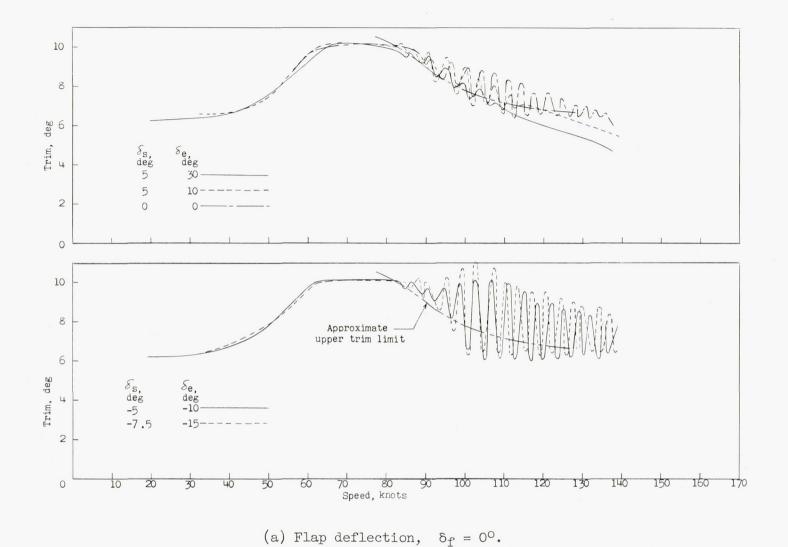
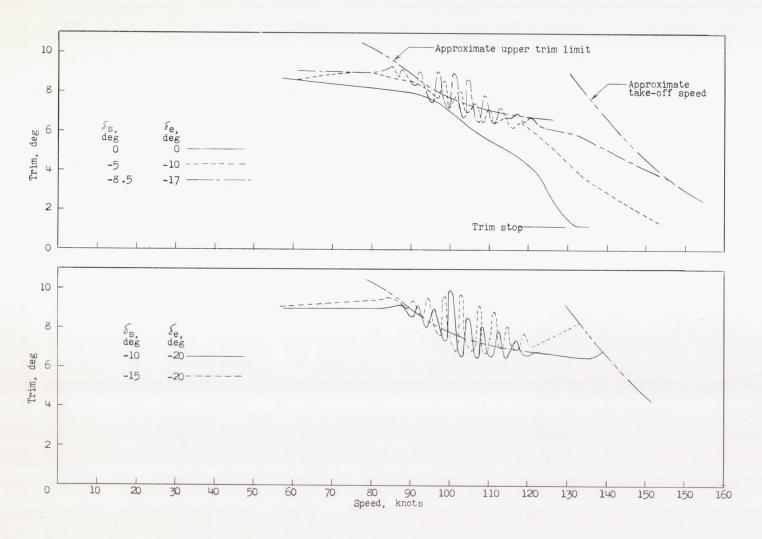


Figure 16.- Variation of trim with speed during take-off in smooth water. Δ_0 = 200,000 pounds; power on.



(b) Flap deflection, $\delta_{\rm f}=40^{\rm o}$.

Figure 16.- Concluded.

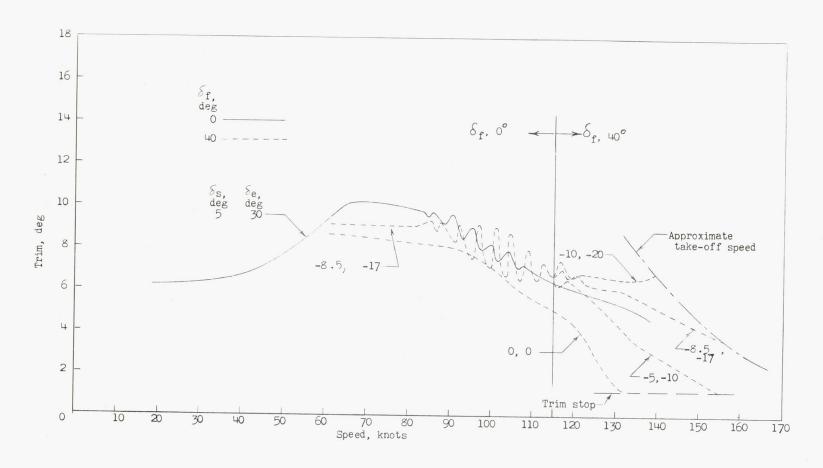
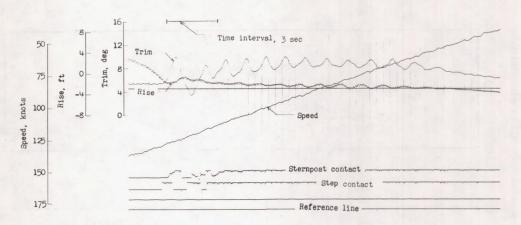


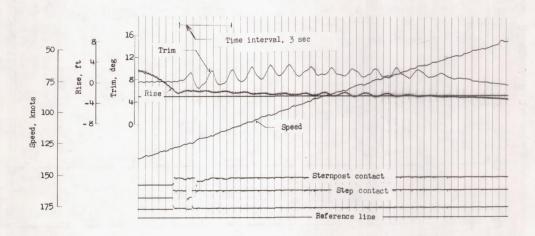
Figure 17.- Variation of trim with speed for two flap deflections showing possible procedures for take-off. Power on.

R





(a) Landing trim, 5.3°.



(b) Landing trim, 7.6°.

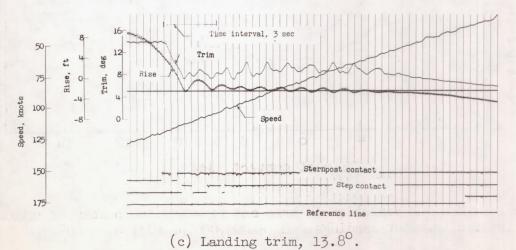


Figure 18.- Typical oscillograph records of landings in smooth water. $\Delta_0 = 200,000$ pounds; $\delta_f = 40^\circ$; power off.





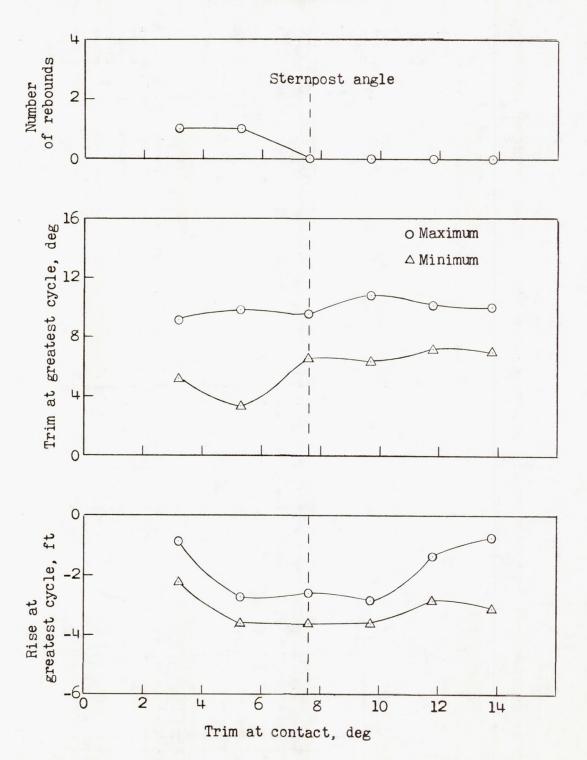


Figure 19.- Maximum variation in trim and rise and the number of rebounds during smooth-water landings. Δ_0 = 200,000 pounds; δ_f = 40°.

